SPRINGBACK PREDICTION OF SHEET METAL IN THE DEEP DRAWING PROCESS USING ELASTOPLASTIC PHENOMENOLOGICAL MODELS

B. Haddag, T. Balan, F. Abed-Meraim
Laboratoire de Physique et Mécanique des Matériaux, ENSAM de Metz, France

Summary

The deep drawing is one of the widely used processes in industry to give suited forms to metal sheets. During deformation the sheet and tools undergo high stresses. The sheet must carry on the deformation until the end of the process. To prevent defects on the final part, like springback or necking, better behaviour models must be used in the numerical simulation. Our work concerns the prediction of springback phenomena using two hardening models written in the frame of phenomenological elastoplasticity. These models were implemented in the ABAQUS finite element software using an accurate, implicit time integration scheme. First, sequential rheological tests have been simulated in order to show the ability of each model to reproduce the effect of strain path changes. Then, an example of deep drawing has been considered to study the effect of the two hardening models on the prediction of springback.

Keywords: elastoplasticity, strain-path, implicit integration, F.E. prediction, deep drawing, springback

1 Introduction

In order to predict the real behaviour of sheet metal under large strain, it is necessary to use an efficient elastoplastic model taking into account the nonlinear strain path history of the material. The sheets are obtained by rolling and thus present anisotropic elastoplastic behaviour. A large class of metals, like the steels considered in our study, exhibits strain path dependent hardening phenomena. We can observe different yield stresses for different loading directions, known as the initial anisotropy, as well as anisotropy induced by work hardening. In the phenomenological elastoplastic models initial anisotropy is modelled by the yield surface and the hardening is decomposed in two parts: isotopic and kinematic. The first part is represented by an expansion of the yield surface and the second part is represented by its translation in the stress space.

For this purpose, two hardening models are considered to model the plastic behaviour: a combined Voce isotropic and Armstrong-Fredericks kinematic hardening model and a microstructural model proposed by Teodosiu and Hu [1] which improves the transient hardening simulation in reverse and orthogonal loading. These two models are coupled with an anisotropic yield criterion to take into account the initial anisotropy. The elasticity is considered linear and isotropic.

Besides modelling, the numerical implementation is an important task to predict correctly the behaviour of industrial parts. Indeed, the quality of numerical results may strongly depend on this task. Consequently, attention is given to study the different integration methods. Implicit time integration of the constitutive equations is recommended by many authors [2] to insure the accuracy and stability of the integration scheme; this is the method we also adopted.

Simulations of rheological tests are first used to show the ability of the two models to reproduce the elementary phenomena observed experimentally. The first model is sufficient to reproduce the Bauschinger effect. On the other hand, the second one is more adequate to reproduce stagnation of work hardening at the beginning of reverse loading and work softening during the orthogonal strain path. Finally, a study of springback during a strip drawing test for a dual phase steel is proposed to show the influence of each model on the final shape obtained after tools removal.

2 Constitutive equations

The two hardening models fit the global frame of classical phenomenological elastoplasticity, governed by the following equations: a constitutive equation relating the elastic strain rate to the stress rate, a yield criterion delimiting the elastic domain, a flow rule defining the inelastic part of the strain rate and then a set of evolution laws for the internal variables defining the work hardening. We first introduce the microstructural model and then obtain the other one as a particular case.

As already stated, the elasticity is considered linear and isotropic. The Cauchy stress rate $\dot{\boldsymbol{\sigma}}$ is related to the elastic strain rate $\mathbf{D}^e$ by the hypoelastic law:

$$\dot{\boldsymbol{\sigma}} = \mathbf{C} : \mathbf{D}^e = \mathbf{C} : \left(\mathbf{D} - \mathbf{D}^p\right) \qquad (1)$$

where the plastic strain rate $\mathbf{D}^p$ is given by the associated flow rule:

$$\mathbf{D}^p = \dot{\lambda} \frac{\partial F}{\partial \boldsymbol{\sigma}} \qquad (2)$$

and the yield criterion is given by:

$$F = \bar{\sigma} - Y = \sqrt{\left(\boldsymbol{\sigma}' - \mathbf{X}\right) : \mathbf{M} : \left(\boldsymbol{\sigma}' - \mathbf{X}\right)} - Y \leq 0 \qquad (3)$$

where $\bar{\sigma}$ and Y are the equivalent stress and the size of the yield surface respectively. The quadratic Hill'48 yield surface is used to model the initial anisotropy. $\boldsymbol{\sigma}'$ is the deviatoric stress, $\mathbf{X}$ is the backstress defining the translation of the centre of the yield surface in the stress space and $\mathbf{M}$ is a fourth order tensor containing Hill's anisotropic

coefficients. According to Teodosiu and Hu [1], Y is given by:

$$Y = Y_0 + R + f|\mathbf{S}| \qquad (4)$$

where R (scalar) and $\mathbf{S}$ (fourth order tensor) are two new internal variables. R describes the contribution of the randomly distributed dislocations to the isotropic hardening and $\mathbf{S}$ describes the directional strength of the persistent planar dislocations structures (PPDS) which is decomposed in an active part S_D (scalar) and a latent part $\mathbf{S}_L$ (fourth order tensor). Another internal variable of this model is the polarity of PPDS described by $\mathbf{P}$ (second order tensor). The evolution equations of the internal variables are summarized below:

$$\dot{R} = C_R\left(R_{sat} - R\right)\dot{\lambda} \qquad (5)$$

$$\dot{\mathbf{X}} = C_X\left(X_{sat}\frac{\boldsymbol{\sigma}' - \mathbf{X}}{\bar{\sigma}} - \mathbf{X}\right)\dot{\lambda} \qquad (6)$$

$$\dot{S}_D = C_{SD}\left[g\left(S_{sat} - S_D\right) - hS_D\right]\dot{\lambda} \qquad (7)$$

$$\dot{\mathbf{S}}_L = -C_{SL}\left(\frac{|\mathbf{S}_L|}{S_{sat}}\right)^{n_L}\mathbf{S}_L\dot{\lambda} \qquad (8)$$

$$\dot{\mathbf{P}} = C_p\left(\mathbf{N} - \mathbf{P}\right)\dot{\lambda} \qquad (9)$$

$$\mathbf{S} = \mathbf{S}_L + S_D\mathbf{N}\otimes\mathbf{N} \qquad (10)$$

where $\mathbf{N} = \mathbf{D}^p \big/ |\mathbf{D}^p|$, X_{sat} is a function of $\mathbf{S}$, while g and h are two scalar functions depending on several internal variables.

To find the first model it is sufficient to consider only the two evolution equations (5) and (6) with X_{sat} as a constant parameter and $Y = Y_0 + R$. Moreover, in equation (6) the direction of saturation for $\mathbf{X}$ is $\mathbf{N}$ rather than $\left(\boldsymbol{\sigma}' - \mathbf{X}\right)/\bar{\sigma}$.

In large strain analysis, the tensorial variable rates must be defined by objective derivatives. We adopt the approach classically recommended for F.E. implementation, where the tensor variables are considered in a rotating frame. In this case, the simple time derivatives acquire the property of objectivity. The rotating frame used in ABAQUS corresponds to the Jaumann rate.

3 Implementation of the models

The weak (integral) form of the equilibrium equation is considered and it is further discretized in finite elements. Then, the contribution to the integral equation is computed for every integration point of all the elements. In displacement-based F.E. codes, the primary unknowns are the displacement increments at each node. Accurate,

incremental kinematical equations are available to compute the corresponding strain increments at the integration points [3]. These two steps are performed by the F.E. code. The strain increment is then considered as driving variable when solving the constitutive equations at each integration point. We focus on the resolution of this local problem, namely the time integration of the constitutive equations. For this purpose we use the implicit time integration scheme for its good accuracy and stability.

The integration is carried out over one increment. First we construct the incremental form of the continuum constitutive equations. The equation of elasticity can be written:

$$\boldsymbol{\sigma}_{n+1} = \boldsymbol{\sigma}_n + \mathbf{C} : \left(\Delta\boldsymbol{\varepsilon} - \Delta\boldsymbol{\varepsilon}^p\right) \qquad (11)$$

where subscripts $n+1$ and n designate the end and the beginning of the current increment while $\Delta(\ )$ designates the increment of the corresponding variable. One has to find $\Delta\boldsymbol{\varepsilon}^p$ and then $\boldsymbol{\sigma}_{n+1}$ satisfying the yield criterion, $F_{n+1} = 0$, when plastic loading occurs. As the plastic strain is of deviatoric nature, it is judicious to decompose $\boldsymbol{\sigma}_{n+1}$ in deviatoric (12) and spherical (13) parts:

$$\boldsymbol{\sigma}'_{n+1} = \boldsymbol{\sigma}'_n + 2G\Delta\boldsymbol{\varepsilon}' - 2G\Delta\boldsymbol{\varepsilon}^p \qquad (12)$$

$$\sigma^s_{n+1} = \tfrac{1}{3} tr\left(\boldsymbol{\sigma}_{\mathbf{n}+1}\right) = \tfrac{1}{3} tr\left(\boldsymbol{\sigma}_{\mathbf{n}}\right) + K tr\left(\Delta\boldsymbol{\varepsilon}\right) \qquad (13)$$

and then solve the plasticity problem in deviatoric space. G and K are the shear and bulk modulus respectively. The spherical part σ^s_{n+1} is completely defined with $\Delta\boldsymbol{\varepsilon}$ but the deviatoric part $\boldsymbol{\sigma}'_{n+1}$ is function of $\Delta\boldsymbol{\varepsilon}^p$, which is an unknown variable given by:

$$\Delta\boldsymbol{\varepsilon}^p = \Delta\lambda \left.\frac{\partial F}{\partial \boldsymbol{\sigma}}\right|_{n+1} = \Delta\lambda \left.\frac{\partial F}{\partial\left(\boldsymbol{\sigma}' - \mathbf{X}\right)}\right|_{n+1} = \Delta\lambda \mathbf{V}_{n+1} \qquad (14)$$

The yield criterion must be satisfied at the end of a plastic increment, i.e.:

$$F_{n+1} = \bar{\sigma}_{n+1} - Y_{n+1} = \bar{\sigma}\left(\boldsymbol{\sigma}'_{n+1} - \mathbf{X}_{n+1}\right) - Y\left(R_{n+1}, \mathbf{S}_{n+1}\right) = 0 \qquad (15)$$

where $\mathbf{S}_{n+1}$, $\mathbf{X}_{n+1}$, R_{n+1} and the others internal variables are obtained by semi-analytical integration of their evolution laws:

$$\mathbf{X}_{n+1} = \mathbf{X}_n e^{-C_X \Delta\lambda} + X^{sat}_{n+1} \frac{\boldsymbol{\sigma}'_{n+1} - \mathbf{X}_{n+1}}{\bar{\sigma}_{n+1}} \left(1 - e^{-C_X \Delta\lambda}\right) \qquad (16)$$

$$R_{n+1} = R_n + \left(R_{sat} - R_n\right)\left(1 - e^{-C_R \Delta\lambda}\right) \qquad (17)$$

$$\mathbf{P}_{n+1} = \mathbf{P}_n + \left(\mathbf{N}_{n+1} - \mathbf{P}_n\right)\left(1 - e^{-C_P \Delta\lambda}\right) \qquad (18)$$

$$S_{D\,n+1} = S_{D\,n} e^{-C_{SD}(g+h)\Delta\lambda} + S_{sat}\frac{g}{(g+h)}\left(1 - e^{-C_{SD}(g+h)\Delta\lambda}\right) \qquad (19)$$

$$\mathbf{S}_{L\,n+1} = \left|\mathbf{S}_{L\,n+1}\right|\frac{\mathbf{S}_{L\,n}}{\left|\mathbf{S}_{L\,n}\right|} = \left(\left|\mathbf{S}_{L\,n}\right|^{-n_L} + n_L\frac{C_{SL}}{S_{sat}^{n}}\Delta\lambda\right)^{-\frac{1}{n_L}}\frac{\mathbf{S}_{L\,n}}{\left|\mathbf{S}_{L\,n}\right|} \qquad (20)$$

$$\mathbf{S}_{n+1} = \mathbf{S}_{L\,n+1} + S_{D\,n+1}\mathbf{N}_{n+1} \otimes \mathbf{N}_{n+1} \qquad (21)$$

$$\left|\mathbf{S}\right|_{n+1} = \sqrt{\left|\mathbf{S}_L\right|_{n+1}^{2} + S_{D\,n+1}^{2}} \qquad (22)$$

For simplicity, the functions g and h are considered constant and equal to their values at the beginning of the increment. Defining another variable $\mathbf{T} = \boldsymbol{\sigma}' - \mathbf{X}$ and noting that $\mathbf{S}_{n+1}$, R_{n+1} are functions only of $\Delta\lambda$, equation (15) can be rewritten as:

$$F_{n+1} = \bar{\sigma}\left(\mathbf{T}_{n+1}\right) - Y\left(\Delta\lambda\right) = 0 \qquad (23)$$

Subtracting equation (16) from (12) and replacing $\boldsymbol{\sigma}'_{n+1} - \mathbf{X}_{n+1}$ by $\mathbf{T}_{n+1}$, we obtain:

$$\mathbf{T}_{n+1} - \boldsymbol{\sigma}'_{n} - 2G\Delta\boldsymbol{\varepsilon}' + 2G\Delta\lambda\mathbf{V}_{n+1} + \mathbf{X}_{n+1} = \mathbf{0} \qquad (24)$$

Since $\mathbf{X}_{n+1}$ and $\mathbf{V}_{n+1}$ are functions of $\mathbf{T}_{n+1}$ and $\Delta\lambda$, the last two equations form a set of non-linear algebraic equations with $\mathbf{T}_{n+1}$ and $\Delta\lambda$ as the only unknowns. The system can be solved by the Newton-Raphson method. After convergence, all variables at the end of increment are updated using equations (12), (13) and (16) to (21).

4 Applications

In this work, we aim to investigate the impact of the hardening models on the simulation of springback. For this purpose, we compare the ability of the selected models to predict the strain-path dependency exhibited experimentally by a mild steel and a dual phase steel. The materials have been provided by the Arcelor and Voestalpine steelmaking companies in the frame of a European project. The material parameters for all the models and materials have been determined and provided by the LPMTM laboratory. For the F.E. simulations, we focus on the dual phase steel since for this material the springback is larger.

4.1 Simulation of rheological tests

A set of typical rheological tests [4] was simulated in order to illustrate the behaviour reproduced by the two hardening models. It consists of a monotonic test (tension or shear), a reverse test (shear Bauschinger) and an orthogonal test (tension followed by shear). We note that all tests are realized on sheet along the rolling direction.

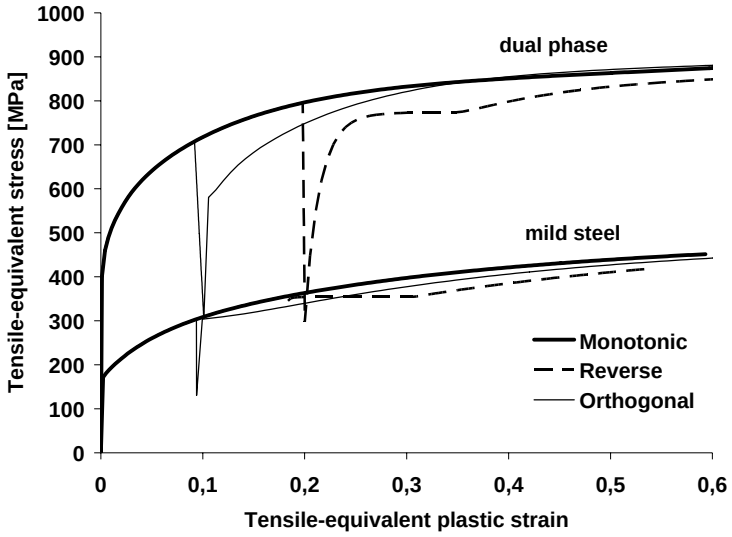

Figure 1: *Simulations with the Teodosiu-Hu hardening model for a mild and a dual phase steels.*

Figure 1 shows the simulation results obtained on dual phase and mild steels represented in terms of equivalent strain and stress. The microstructural model is more accurate in that sense it represents well the transient hardening after strain path change i.e. the stagnation of work hardening at the beginning of reverse shear and hardening followed by softening in the orthogonal test.

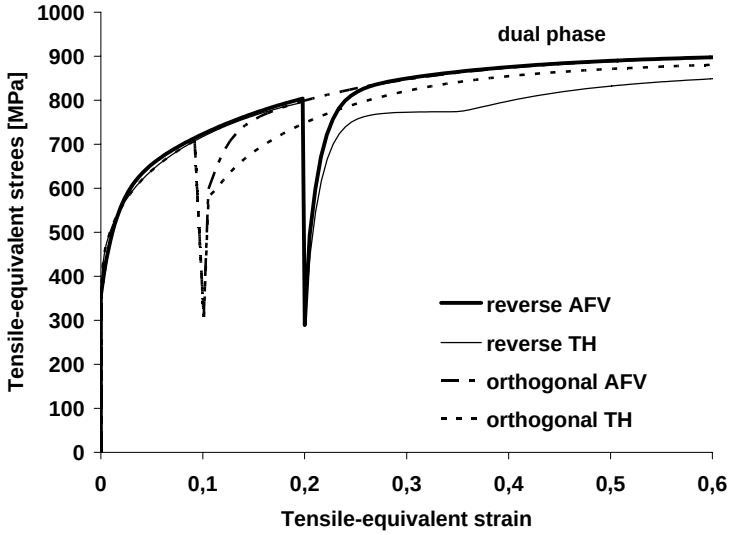

Figure 2: *Simulations with Teodosiu-Hu (TH) and Armstrong-Fredericks-Voce (AFV) hardening models for a dual phase steel*

Figure 2 represents the results obtained for dual phase steel with the two hardening models. The comparison shows that the flow stress is overestimated when strain path

change occurs with the combined Voce isotropic and Armstrong-Fredericks kinematic hardening model. The simulations with the microstructural model are shown very close to the experimental behaviour [4].

4.2 Springback simulation for a strip drawing test

In order to investigate the effects of the hardening models on the springback of a dual phase sheet steel, the strip drawing benchmark test, initially proposed at NUMISHEET'93, was selected with modified dimensions. The sheet has 1.2 mm thickness, 450 mm length and 45 mm width. The die radius (3.25 mm) and the punch radius (3 mm) are much smaller than in the initial benchmark. The blank holder force has the magnitude of 84 KN. The friction coefficient between the tools and the sheet was assumed constant with 0.075.

The problem is treated in 2D. The blank is meshed in ABAQUS/standard with four rows of 2D solid finite elements CPE4IH. The tools are rigid.

The convergence difficulties due to contact evolution may be avoided by simulating the forming step with a dynamic explicit code [5]; the results are then transferred to an implicit code to simulate the springback step (tools removal). Here, we simulate all steps with the implicit code (ABAQUS/standard) via the UMAT routine. This allows us to verify more accurately the equilibrium state during the forming stage.

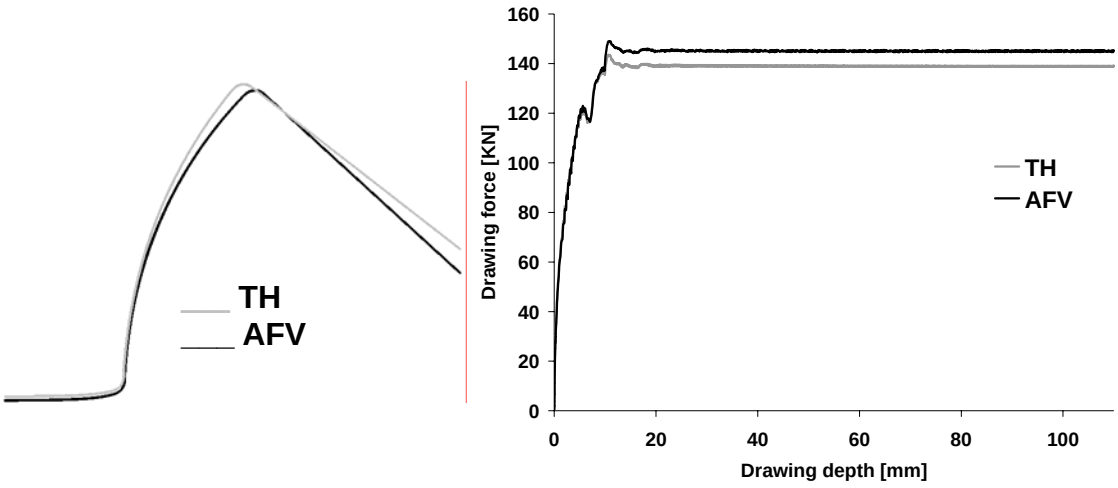

Figure 3: *Deformed shapes obtained with the two models and the corresponding punch reaction forces.*

Figure 3 shows the two deformed shapes obtained with our selected models. The amount of springback can be measured by the angle between the initial and the final positions of the flange or the curvature radius of the sidewall. From **Figure 3**, it appears that the amount of springback is overestimated with the first (classical) model. The interpretation of this result can be found in the **Figure 2**. It indicates that in the

subsequent strain path (orthogonal or reverse) the microstructural model gives a lower flow stress than the one given by the classical model. Thus, if an elastic unloading occurs at the same configuration the elastic strain part will be lower for the microstructural model than for the first model. These observations are confirmed experimentally: the high strength sheet metals exhibit generally a high springback. As another consequence of the different strain-path sensitivity, the punch reaction force is overestimated with the first model (**Figure 3**).

5 Conclusions

Several parameters influence springback. In this study, the influence of the hardening models is studied and outlined. The strain-path dependency of the hardening models is shown as one of the important factors to consider in the elastoplasticity models in order to predict accurately the final shapes of industrial parts.

6 Acknowledgements

This work has been carried out in project funded by the European Commission, Research Fund for Coal and Steel (contract 7210-PA/371). The strip drawing test geometry has been suggested by Dr. Edwin Till from Voestalpine, Austria. The authors are grateful to Prof. Cristian Teodosiu from LPMTM (Univ. Paris 13) for fruitful discussions and guidance during this work.

7 References

[1] Teodosiu, C. and Hu, Z.: Evolution of the intragranular microstructure at moderate and large strains: Modelling and computational significance, Simulation of Materials Processing: Theory, Methods and Applications, Proc. of Numiform'95, (1995), 173-182.

[2] Ortiz, M. and Popov, E. P.: Accuracy and stability of integration algorithms for elastoplastic constitutive relations, International Journal for Numerical Methods in Engineering, Vol. 21(1984), 1561-1576.

[3] Hughes, T.J.R.: Numerical implementation of constitutive models: rate-independent deviatoric plasticity, in Theoretical foundation for large-scale computations for nonlinear material behavior, Martinus Nij Publishers, Netherlands, (1984), 29-57.

[4] Bouvier, S., Teodosiu, C., Haddadi, H., Tabacaru, V.: Anisotropic work-hardening behaviour of structural steels and aluminum alloys at large strains, Journal de Physique IV Vol. 105, (2003), 215-222.

[5] Lee, M.-G., Kim, C., Kim, C., Wenner, M. L. and Chung, K.: Springback evaluation of automotive sheets based on isotropic-kinematic hardening laws and non-quadratic anisotropic yield functions, International Journal of Plasticity, Vol. 21(2005), 915-953.